Cognitive Robotics 3 (2023) 93–106

Contents lists available at ScienceDirect

Cognitive Robotics

journal homepage: http://www.keaipublishing.com/en/journals/cognitive-robotics/

Adjustable Convergence Rate Prescribed Performance with Fractional-Order PID Controller for Servo Pneumatic Actuated Robot Positioning

Mohd Iskandar Putra Azahar, Addie Irawan*, R.M.T. Raja Ismail

Robotics, Intelligent Systems & Control Engineering (RiSC) Research Group, Faculty of Electrical & Electronics Engineering Technology, Universiti Malaysia Pahang, 26600 Pekan, Pahang, Malaysia

ARTICLE INFO

Keywords:
Pneumatic actuator
adjustable convergence rate
finite-time prescribed performance control
pneumatic robot

ABSTRACT

This study presents the method for optimal error tracking in position control for a servo pneumatic actuated robot grasper system using a new adjustable convergence rate prescribed performance control (ACR-PPC). It focuses on improving the feedback controller and the fractional-order proportional-integral-derivative (FOPID) controller used for the position control of each robot's finger. Multiple features were considered such as tracking error, rising time, faster transient response with finite-time convergence, oscillation reduction, and pressure stabilization in the pneumatic system. Experiments were conducted using a single finger of a tri-finger pneumatic gripper (TPG) robot, actuated by a single proportional valve with a double-acting cylinder (PPVDC). Two types of input trajectories were tested: step and sine wave inputs, which are common and critical for pneumatic systems. The results show that the proposed method eliminates oscillation and achieves high tracking performance within the prescribed bounds and minimal overshoot as well. The oscillation was suppressed with minimal overshoot and fast response was achieved by tuning the formulated adjustable prescribe performance function, thus improving the rising time response without significant loss of performance.

1. Introduction

Pneumatic and hydraulic systems, known as fluid dynamic actuators, are widely used in various industrial fields around the world due to their high power-to-weight ratio and reliability. Pneumatic actuators offer advantages over hydraulic actuators in terms of cleanliness, simplicity of design, low cost, and immunity to electromagnetic interference. However, the compressibility of air results in a lower natural frequency in pneumatic systems, making the airflows more complicated through valve pipeline and challenging to enhance positioning and tracking accuracy. Additionally, the nonlinear and unpredictable behavior of pneumatic systems is caused by the presence of frictional forces, making the control of motion in pneumatic servo systems (PSS) a challenging task. To achieve stability

List of abbreviations: PSS, Pneumatic Servo System; FLC, Fuzzy Logic Control; PPVDC, Pneumatic Proportional Valve with a Double-Acting Cylinder; TPG, Tri-Finger Pneumatic Gripper; PID, Proportional Integral and Derivative; FOPID, , Fractional-order PID; FO, Fractional Order; PPC, Prescribed Performance Control; PPF, Prescribed Performance Function; ARC-PPC, Adjustable Convergence Rate Prescribed Performance Control; AC-PPF, Adjustable-Convergence Rate PPF; CPPC, Conventional Prescribed Performance Control; P+ID, Proportional Plus Integral and Derivative; PSO, Particle Swarm Optimization; AHU, Air Handling Unit; MISO, Multiple Input and Single-Output; MCU, Microcontroller Unit; GS, Gripping State; RS, Release State; IAE, Integral Absolute Error; ISE, Integral Square Error; ITAE, Integral Time Absolute Error.

* Corresponding author.
E-mail address: addieirawan@ump.edu.my (A. Irawan).

https://doi.org/10.1016/j.cogr.2023.04.004
Received 16 March 2023; Received in revised form 14 April 2023; Accepted 14 April 2023
Available online 27 April 2023

List of Symbols

ϑ_a	Decay Function
ρ	Predefined Performance Function
ρ_o	Initial Value of the Tracking Error at the Transient Interval
ρ_∞	Maximum Allowable Range of the Tracking Error at the Steady-state Interval
t_0	Predefined Convergence Time
ψ	Adjustable Prescribed Function
$\beta_{i(i=1,2)}$	Scaling Factor
h	Convergence Rate
$\bar{\sigma}$	Upper Boundary Gain of the PPC
$\underline{\sigma}$	Lower Boundary Gain of the PPC
$\bar{\sigma}\rho(0)$	Upper Limit of the Maximum Overshoot
$\underline{\sigma}\rho(0)$	Lower Limit of the Maximum Undershoot
$\varepsilon(t)$	New Transformed Tracking Error
x_d	Reference Input of Displacement for the Rod-Piston Stroke
$e(t)$	Tracking Error
x_{rp}	Feedback Response of Displacement for the Rod-Piston Stroke
K_p	Proportional Gain of the FOPID Controller
K_i	Integral Gain of the FOPID Controller
K_d	Derivative Gain of the FOPID Controller
λ	Integral Order of the FOPID Controller
μ	Differential Order of the FOPID Controller

and efficiency in the face of these challenges, a strong control strategy for pneumatic systems is crucial. Significant efforts have been put forth to enhance control systems for pneumatic actuators, specifically to control the position of rod-piston by utilizing numerical control theories, intelligent systems, and optimization techniques that are based on computing. Many different control strategies have been developed to address the issues in PSS, including the combination of classical control systems, as well as integrated approaches incorporating modern techniques such as cascading proportional integral derivative (PID) control, adaptive fractional-order control, intelligent control, and data-driven control as well through computing method. Despite their potential, these feedback controllers alone struggle to perform effectively in nonlinear systems with uncertainties, like PSS. Prescribed performance control (PPC) [1,2] architecture has recently gained popularity due to its simplicity, allowing the user to set error boundary parameters to enhance feedback control performance. However, conventional PPC has some drawbacks such as the lack of finite time features and a fixed convergence boundary, which limits its practical applications in real-time scenarios.

Therefore, this study presents a method to optimize the pneumatic position control system using a newly formulated adjustable convergence rate prescribed performance control (ACR-PPC). The focus of this study is to address the high nonlinearities inherent in the servo pneumatic rod-piston position control of a single proportional valve with a double-acting cylinder (PPVDC), attached to each finger of the tri-finger pneumatic grippers (TPG) robot. The fractional-order proportional-integral-derivative (FOPID) controller is used as the feedback control platform, which is improved by the proposed ACR-PPC because it is currently used as the core closed-loop controller for each finger proportional motion in the TPG system. Additionally, this study addresses the dynamic stability and unmeasurable test rig constraints such as frictional force at the joint, slip at the joint, and the gravity force factor of the PPVDC. Experiments were conducted using two types of input trajectories: step and sinusoidal inputs, which are considered common, practical, and critical inputs for a PPVDC motion [3].

In this paper, Section II covers the discussion on related works regarding control system design and solutions for pneumatic systems. Section III provides information on the pneumatic actuated robot system and its operating principles that were used in this study. Section IV outlines the methodology of the proposed ACR-PPC design, its formulation, and its integration with the FOPID controller as the inner-loop controller. The results of experiments conducted using the TPG robot platform and their analysis are presented in Section V, and the paper concludes with Section VI.

2. Related Works in the Design and Solution of Control Systems for Pneumatic Systems

A substantial rise in the use of pneumatic actuators in industrial automation has been noted particularly in the applications such as machine precision and flexible systems (robot manipulators and intelligent vehicles). This has led to an increased demand for accurate position tracking performance and consistent positioning between the two endpoints of the pneumatic actuator's stroke [3,4]. Furthermore, computational intelligence integrated with optimization strategy approaches are gaining traction as a solution, particularly in improving the performance of control systems. The function approximation-based intelligent design strategy is commonly recognized as a prominent way to cope with the unknown nonlinearities and uncertainties. For instance, fuzzy logic control with cascade strategy approach was used by [5], whereby the single-input fuzzy P+ID controller was proposed for the dynamics control with hysteresis compensation on the soft-pneumatic actuator. Fuzzy logic was also used by Chojecki and Ambroziak in their works

Table 1
List of equipment

Equipment	Value
Pneumatic cylinder	CKD Air Cylinder CAC4-A-50B-75-Y/Z
Pneumatic proportional valve	Festo MPYE-5-1/4-010-B
Pneumatic pressure regulator & filter	AirTAC SR200
Pneumatic pressure transducer	Festo SPTW-P10R-G14-A-M12
Air compressor	SWAN SVP202 Air Compressor
Rotary encoder	Rotary encoder - 500ppr

as self-tuning tools for particle swarm optimization (PSO) algorithm in air handling unit (AHU) equipped with multiple actuators [6]. The similar fuzzy logic-based self-tuning approach was also deployed in [3,7] using a hybrid strategy for a PSS in robot system. However, an adaptive neural network was used to improve the performance of error tracking control on PSS in [8]. Most of the integration approaches perform an impressive tracking performance of more than 70% whenever compared to the conventional control method without any intelligent system assistance. However, most of these systems are still in the offline and predetermined practices which require further refining in the real-time process to cater the unpredictable conditions.

In recent years, a lot of research on fractional order (FO) control systems has been conducted. Unlike traditional calculus which uses integer orders of derivatives and integrals, fractional order calculus uses real-number orders. Integer-order derivatives and integrals are just special cases of their fractional-order equivalents. In [9], a fractional-order disturbance observer was proposed to estimate mismatched disturbances, while a novel fractional-order sliding mode controller based on an observer was proposed to reduce tracking inaccuracies and chatter. For instance, in [10], an adaptive sliding mode control was improved with a fractional-order derivative sliding surface and a switching-type reaching law, leading to less chattering and reduced energy consumption for targeted PSS. On the other hand, discrete-time FO integral sliding mode control approach, proposed by [11], was developed to stabilize pneumatic artificial muscles with an antagonistic configuration, using a fractional-order exponential reaching law. FO approaches also done by [5,12], whereby two solutions were proposed using FO integral sliding surfaces and different reaching rules to reduce reaching time and improve system performance. Researchers have also integrated FO systems with other control systems such as intelligent control systems to increase the dimensionality of the FO system. For example, a two-degree-of-freedom FO fuzzy PID controller was proposed to improve PSS accuracy in [13]. The FOPID controller provides a significant advantage over a typical PID controller by having two additional tunable parameters. However, with more parameters, the tuning process is more difficult, especially if it was done manually.

In 2008, Bechlioulis introduced and published a prescribed performance control (PPC), a new control approach with output constraints that guarantees system output convergence and crucial signal responses such as maximum overshoots and steady-state error into an infinitely narrow prescribed area. In other words, PPC acts as a conjunction between the controller input and the controller itself [2]. PPC has been employed in a wide range of control engineering applications that require output restrictions [14,15]. The primary objective of PPC was to keep the transforming error function within a specified range to attain the satisfaction of the prescribed error performance metrics for the tracking error [16]. A new proportional-integral approximation-free control for nonlinear robotic systems using PPFs without utilizing any function approximate solution was developed in [17]. This approach was further improved with a low-complexity structure and prescribed input constraints in [18]. An adaptive control approach with PPF restrictions was established in [19] to stabilize the vertical and pitch displacements in active suspensions despite parametric uncertainties. An adaptive control technique was developed in [20] to ensure the convergence of tracking error and limit maximum overshoot in the suspension system with PPF restrictions and in case of actuator malfunction. However, these results rely on the assumption that all system parameters are observable or can be immediately quantified, which is unlikely to happen in practical implementations [14], and external disturbances can negatively impact control effectiveness [21]. For time-delay systems with PPF limitations, an output-feedback control approach was proposed in [22], while a dynamic surface control technique in response to the increasing complexity of problems was introduced in [23].

According to the non-restricted characteristic in the PPC method, numerous feedback control techniques can be utilized with this conjunction control system to enhance and optimize its feasibility especially with the nonlinear plant. Furthermore, the PPF allows users to pre-define the performance constraint parameters on the control system and obtain the guaranteed performance for limiting the tracking error to within a prescribed boundary region. This method has potential to replace or reduce the need of approximation control approaches to cater the uncertainties in nonlinear control system structure such as position control on PSS.

3. Pneumatic Actuated Robot System and Its Principle of Operation

This section provides a comprehensive overview of the working principle of the tri-finger pneumatic gripper (TPG) system. The TPG platform consists of three independently actuated pneumatic actuators as illustrated in Fig. 1. The robot grasper operates in two primary states: (1) the gripping state (GS) and (2) the release state (RS). The GS state can be proportioned up to the maximum point as shown in Fig. 1(a), and vice versa for the RS state as shown in Fig. 1(b).

Each rod-piston pneumatic cylinder has a length of 75 mm, with a particular emphasis on the positioning of one rod-piston for one finger. The main components of the platform are displayed in Table 1. The control system design for this platform uses a multiple input and single output (MISO) configuration and is implemented using a 32-bit microcontroller unit (MCU) running a real-time

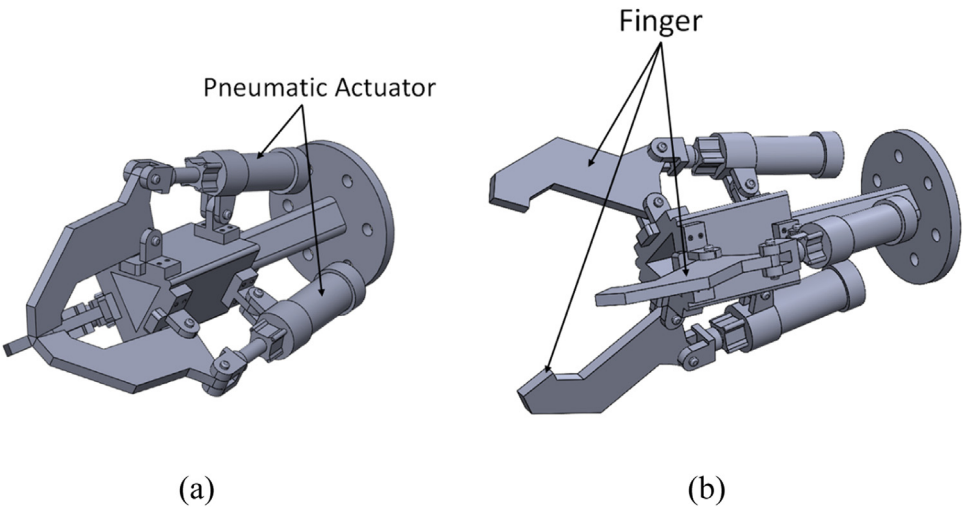

Figure 1. TPG in (a) gripping state and (b) release state.

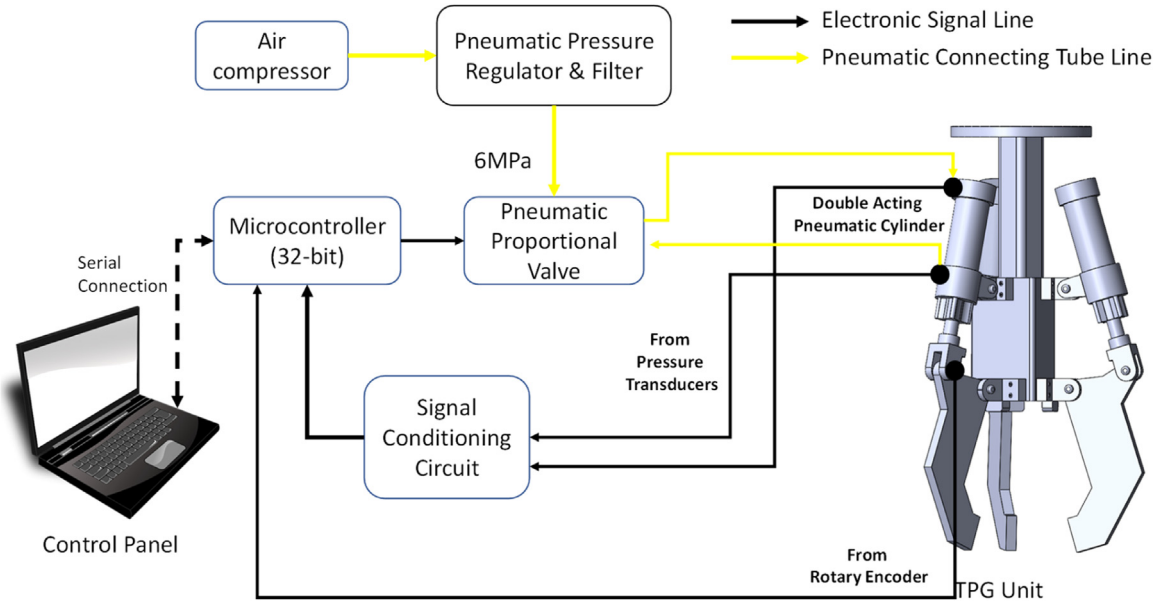

Figure 2. Schematic diagram for the hardware connection of a single finger of TPG robot

operating system. The MCU controls each rod-piston of each finger in the TPG robot through a proportional valve and considers minimum two feedback signals, from the rotary encoder on the finger joint and the pressures from each pneumatic piston cylinder to perform closed-loop control. The hardware schematic of the TPG robot control for a single finger connection is shown in Fig. 2.

4. Controller Design

4.1. Adjustable Converge Rate Prescribed Performance Control

A limitation has been identified in the finite-time prescribed performance function proposed and deployed in [24–26], where the convergence rate is fixed. The concept of an adjustable convergence rate presents a more promising solution to overcome the limitations of a fixed rate, as introduced in [2]. This allows for the ability to vary and adjust or tune either the finite time of convergence rate or the different transient rate settings. Therefore, the new adjustable convergence rate PPF (AC-PPF) formulation is introduced as Eq. (1) as follows:

$$\rho(t) = \left(\rho_0 - \rho_\infty\right)\vartheta_a + \rho_\infty \tag{1}$$

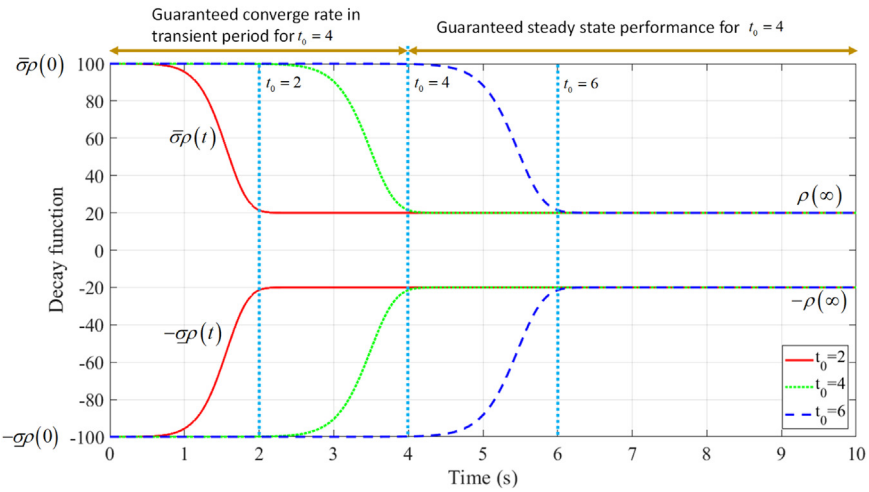

Figure 3. Example of mechanism of the AC-PPF for adjustable finite time

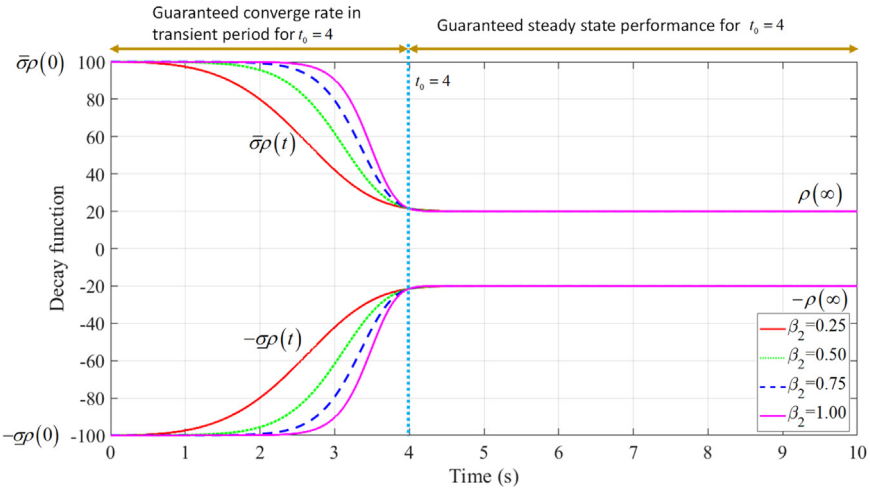

Figure 4. Example of mechanism of the AC-PPF for adjustable converge rate

where the specified performance function or smooth function $\rho(t)$ is decreased strictly and $\lim_{t\to\infty}\rho(t) = \rho_\infty$. ρ_o represents the initial value of the tracking error $e(t)$ at the transient interval. On the other hand, ρ_∞denotes the maximum permissible range of the $e(t)$at the steady-state interval, in which $\rho(t),\rho_0 > \rho_\infty > 0$. The parameter $h > 0$ represents the convergence rate speed of the. Therefore, as shown in illustration from the simulations in Fig. 3 and 4, $\bar{\sigma}$, $\underline{\sigma}$, h, ρ_0, and ρ_∞ can be tuned to improve both transient and steady-state performances [26]. The decay smooth function, ϑ_a, is modify as Eq. (2) as follows:

$$\vartheta_a = e^{-\frac{\psi(t)^2}{{t_0}^2}} \tag{2}$$

where,

$$\psi(t) = \beta_1 t\left(\tanh\left[\beta_2\left(t - t_0\right)\right] + 1\right) \tag{3}$$

where t_0 is the predefined convergence time,β_1 is the scaling factor for finite time with the default value of 1, and β_2 is the scaling factor of converging rate with the default value of 1. The first advantage of AC-PPF is its ability to adjust the finite-time convergence rate, as demonstrated through simulation as shown in Fig. 3. It can be seen that t_0 can be altered through manipulation of $t_0 = 2$, $t_0 = 4$, and $t_0 = 6$. Furthermore, the second feature of AC-PPF is the capability to modify the transient period of the convergence rate by selecting the value β_2 as depicted in simulation of the function as shown in Fig. 4 with $\beta_1 = 1$ by default. The convergence rates are different for different value of β_2, whereby the convergence curve earlier by the decreasing of β_2 value.

Remark 1: $e(t)$and $\bar{\sigma}, \underline{\sigma}$ are both positive finite values. Additionally, both $\bar{\sigma}\rho(0)$ and $\underline{\sigma}\rho(0)$ symbolize the upper limit of the maximum overshoot and the lower limit of the undershoot, respectively.

4.2. Error Transformation

For the control scheme with a PPF constraint, the prescribed performance boundary is transformed into an equality form through an output transformation. To achieve this, a smooth and strictly increasing function $S[\varepsilon(t)]$ is introduced, as expressed in Eq. (4) as follows:

$$S[\varepsilon(t)] = \frac{\bar{\sigma}e^{\varepsilon(t)} - \underline{\sigma}e^{-\varepsilon(t)}}{e^{\varepsilon(t)} + e^{-\varepsilon(t)}}. \tag{4}$$

Remark 2: $S[\varepsilon(t)]$ satisfies

1 $-\underline{\sigma} < S[\varepsilon(t)] < \bar{\sigma}$
2 $\lim_{\varepsilon(t)\to+\infty} S[\varepsilon(t)] = \bar{\sigma}, \quad \lim_{\varepsilon(t)\to-\infty} S[\varepsilon(t)] = -\underline{\sigma}$

To establish the relationship between $e(t)$ and $\rho(t)$, the initially defined constraint tracking error is transformed into an unconstrained form through error transformation methods, allowing the performance condition to be represented as in Eq.(5) as follows:

$$e(t) = \rho(t)S[\varepsilon(t)]. \tag{5}$$

The parameter of $\varepsilon(t)$ is developed to the increased function, $S[\varepsilon(t)]$ and $e(t) < \rho(t), \forall t \geq 0$ is obtained because the function of $S[\varepsilon(t)]$ is strictly monotonic increasing. The behavior of bounds on both steady-state and transient responses can be ensured by defining $\rho(t)$ properly. The function that defines the inverse transformation for the bounded $\varepsilon(t)$and represents a newly transformed adjustable tracking error can be expressed as Eq. (6) as follows:

$$\varepsilon(t) = S^{-1}\left(\frac{e(t)}{\rho(t)}\right) = \frac{1}{2}\ln\left(\frac{\psi(t)+\underline{\sigma}}{\bar{\sigma}-\psi(t)}\right) \tag{6}$$

where $S^{-1}(\bullet)$ is the inverse function of $S(\varepsilon)$. Meanwhile, $\psi(t) = e(t)/\rho(t)$ is a normalized error and $|\varepsilon(0)| < 1$. According to [26], if $\varepsilon(t) \neq 0$, $\psi(t)$ satisfies the condition $-1 < \psi(t) < 1$. Furthermore, the predefined bound of PPF is guaranteed whenever $\varepsilon(t)$ is constantly bounded. The time derivative of $\varepsilon(t)$and the following function can be obtained as follows:

$$\begin{aligned}\dot{\varepsilon}(t) &= \tfrac{1}{2}\left[\tfrac{1}{\psi(t)+\underline{\sigma}} - \tfrac{1}{\psi(t)-\bar{\sigma}}\right]\left[\tfrac{\dot{e}(t)}{\rho(t)} - \tfrac{e(t)\dot{\rho}(t)}{\rho^2(t)}\right] \\ &= r_i\left[\dot{e}(t) - \tfrac{e(t)\dot{\rho}(t)}{\rho(t)}\right]\end{aligned} \tag{7}$$

where,

$$r_i = \frac{1}{2\rho}\left[\frac{1}{\psi(t)+\underline{\sigma}} - \frac{1}{\psi(t)-\bar{\sigma}}\right] \tag{8}$$

Remark 3: The system's state is transformed through the smooth function $S[\varepsilon(t)]$outlined in Eq. (4) and ensuring the regulation of the input reference from the stability of $e(t)$in accordance with the performance constraint described in Eq. (1).

Remark 4: PPF constraint Eq. (1) and error transform $S[\varepsilon(t)]$ are proposed for the control design process by choosing the control parameters $\bar{\sigma}$, $\underline{\sigma}$, t_0, $\lambda_1, \lambda_2, \rho_0$, and ρ_∞. Since the parameters $\bar{\sigma}$, $\underline{\sigma}, \rho_0$, and ρ_∞ are selected so that the initial condition $-\underline{\sigma}\rho(0) < e(0) < \bar{\sigma}\rho(0)$ is satisfied and $\varepsilon(t)$ can be restricted within the boundaries, the condition $-\underline{\sigma} < S[\varepsilon(t)] < \bar{\sigma}$ is held. Therefore, the control problem under the condition $-\underline{\sigma}\rho(t) < e(t) < \bar{\sigma}\rho(t)$ is guaranteed.

4.3. Integration of ACR-PPC to the FOPID Controller

As mentioned earlier, $PI^{\lambda}D^{\mu}$ or FOPID controller [27] is used as a nominal feedback control or inner controller platform to verify the proposed ACR-PPC system. The general equation for a FOPID controller is expressed as Eq. (9) as follows:

$$u(t) = K_p e(t) + K_{it_0} {I_t}^{-\lambda} e(t) + K_{dt_0} {D_t}^{\mu} \dot{e}(t) \tag{9}$$

where K_p, K_i, and K_d are the proportional, fractional integral, differential gains coefficient, respectively. The tracking error of the system is defined by$e(t) = x_d(t) - x_{rp}(t)$, where $x_d(t)$ and$x_{rp}(t)$ are both trajectory input reference and feedback response for the rod piston of PPVDC, respectively. Additionally, two constant parameters, λ and μ, represent the integral and differential orders, respectively, which are the extra tuning parameters from the FOPID controller. Table 2 displays a typical FOPID controller, which greatly expands the versatility of PID control design. The general formula for the FOPID controller to track the position error of the PPVDC can be derived as Eq. (10) as follows:

$$u(t) = P(t)e(t) + I^{\lambda}(t)e(t) + D^{\mu}(t)e(t) \tag{10}$$

with

$$P(t) = K_p e(t) \tag{11}$$

and

$$I^{\lambda}(t) = K_i R_i(t) \tag{12}$$

Table 2
List of FOPID controller with extra parameters setting

Controller	Control Parameters
P	$\lambda = 0, \mu = 0$
PI	$\lambda = 1, \mu = 0$
PD	$\lambda = 0, \mu = 1$
PID	$\lambda = 1, \mu = 1$

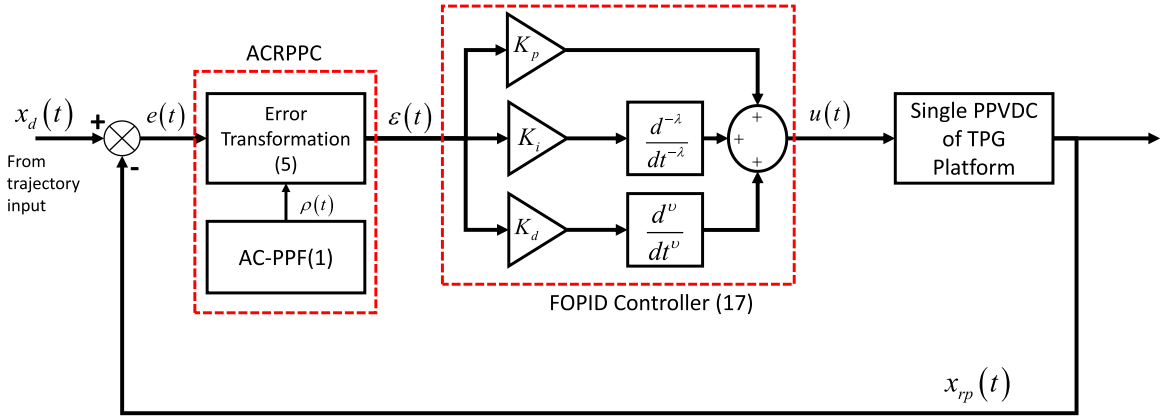

Figure 5. The block diagram of ACR-PPC with FOPID controller to a single PPVDC rod-piston of the TPG robot

where both $K_i$and $R_i(t)$are as follows:

$$K_i = \frac{K_p}{T_i} \tag{13}$$

$$R_i(t) = {}_{t_0}D_t^{-\lambda} e(t) = \frac{1}{\Gamma(\lambda)} \int_{t_0}^{t} (t-\tau) f(\tau) d(\tau) \tag{14}$$

for the D^{μ} in Eq.(10), it can be expressed as follows:

$$D^{\mu}(t) = K_d R_d(t) \tag{15}$$

where,

$$K_d = K_p T_i \tag{16}$$

$$R_d(t) = {}_{t_0}D_t^{\mu} e(t) = \frac{1}{\Gamma(m-\mu)} \frac{d^m}{dt^m} \int_0^t (t-\tau)^{-\mu+m-1} e(\tau) d(\tau) \tag{17}$$

For the integration with ACR-PPC, Eq. (10) can be rephrased by substituting Eq. (6) into the equation, thus, the new control input design with error transformation can be expressed as Eq. (18) as follows:

$$u(t) = P(t)\varepsilon(t) + I^{\lambda}(t)\varepsilon(t) + D^{\mu}(t)\varepsilon(t) \tag{18}$$

The complete design of the ACR-PPC with the FOPID controller is depicted in Fig. 5. It encompasses the ACR-PPC and FOPID control structures, as well as a single pneumatic actuation component in the form of the TPG platform serving as the plant.

5. Results and Discussions

The proposed control technique was evaluated through experimental studies using the TPG robot platform. The test setup is shown in Fig. 6. The experiments were conducted with two crucial types of input trajectories for a single PPVDC unit that drives a TPG finger: (1) step input and (2) sinusoidal input. The step input was designed to evaluate the performance of the proposed controller with a focus on fast response, while the sinusoidal input was used to evaluate the control strategy's ability to reduce the constant time lag or phase delay between the desired input and feedback response. Both inputs performed GS and RS operations on the targeted TPG finger with different speeds and motion periods.

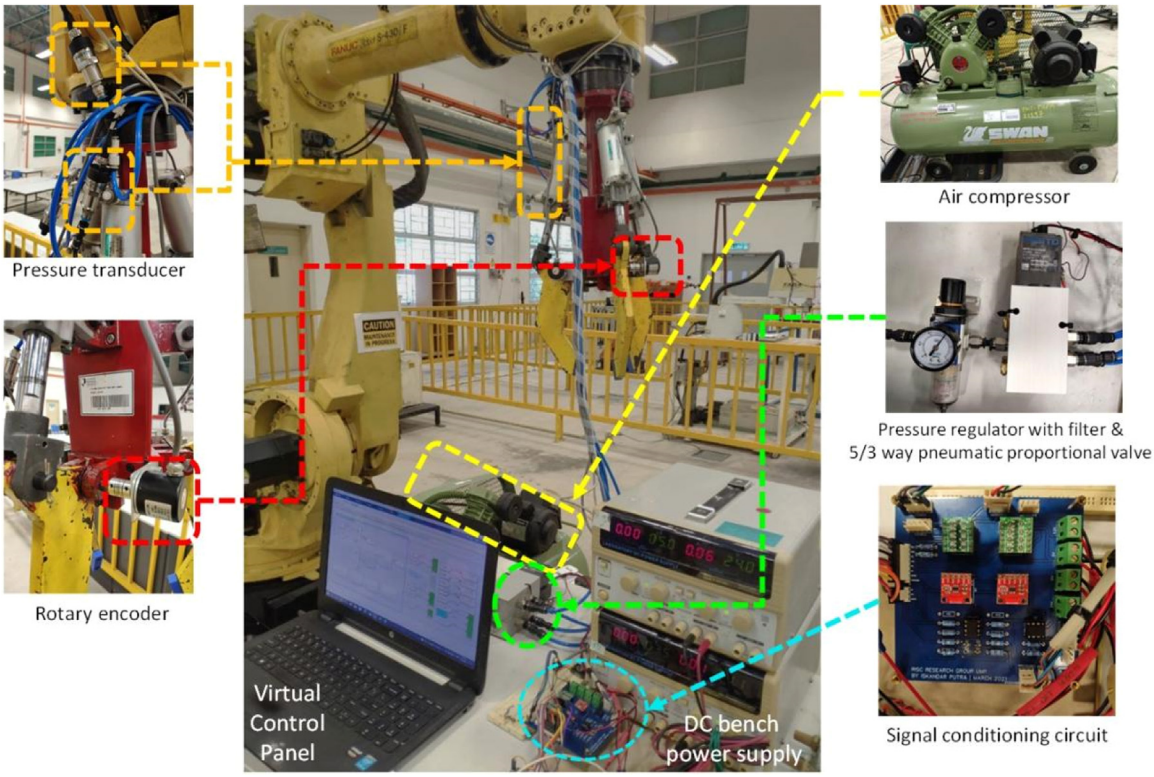

Figure 6. Experimental Setup

Table 3
Controller parameters for step input trajectory test

Controller	Parameters	Value
FOPID (a), (b)	$K_p, K_i, K_d, \lambda, \mu$	435, 68, 7, 0.5, 0.2
ACRPPC-FOPID (a)	$K_p, K_i, K_d, \lambda, \mu,$ $\rho_0, \rho_\infty, \bar{\sigma}, \underline{\sigma}, t_0, \lambda_1, \lambda_2$	65, 0.55, 0.81, 9, 0.1, 50,4,1,1,0.3,1,3
ACRPPC-FOPID (b)	$K_p, K_i, K_d, \lambda, \mu,$ $\rho_0, \rho_\infty, \bar{\sigma}, \underline{\sigma}, t_0, \lambda_1, \lambda_2$	65, 0.55, 0.81, 9, 0.1, 50,4,1,1,0.3,1,3

5.1. Step Input Trajectory Test

For this test, a step input trajectory was implemented within a range of 0to 30 mm for the pneumatic cylinder. Table 3 shows the finetuned controller parameters for both FOPID and PPCs for the step input trajectory. To test the ACR-PPC's ability to converge at a user-defined finite time, two conditions of trajectory initial input steps were run. These conditions involved a step input starting at either 0 or 4 s, with a desired piston position of 30 mm. These two input trajectory conditions were conducted to verify the potential of ACR-PPC compared to C-PPC, which is unable to achieve finite-time convergence.

Fig. 7 shows that the ACRPPC-FOPID controller exhibits superior stability, precision, and absence of overshoot compared to the FOPID and CPPC-FOPID controllers in the step input positioning. The ACRPPC-FOPID controller has a 25% faster rise time compared to the CPPC-FOPID controller, resulting in improved stability of the positioning control. The FOPID controller has a slightly quicker transient response, it was unable to effectively address the overshoot problem, as demonstrated at around 0.2 s as shown in Fig. 7(a). The ACRPPC-FOPID controller has a 7% and 5% faster settling time compared to the FOPID and CPPC-FOPID controllers, respectively. This trend can also be seen in the initial operation starting at 4 ss as shown in Fig. 7(b). In this scenario, the ACRPPC-FOPID controller exhibits significantly more stability and control compared to the CPPC-FOPID and FOPID controllers in terms of steady state error. Meanwhile, the CPPC-FOPID controller exhibits a large steady state error after about 1.8 s of hold, with an error range of 2.5 to 5 mm, compared to the ACRPPC-FOPID and FOPID controllers.

From the perspective of prescribed performance, the tracking error of the rod-piston system using CPPC-FOPID and VPP-FOPID controllers is shown in Fig. 8. The tracking error from the FOPID controller was also included for comparison. As seen in Fig. 8, despite operating within the prescribed bounds, the FOPID controller still experienced oscillations early on compared to the CPPC-FOPID and ACRPPC-FOPID controllers. Fig. 8(a) demonstrates the advantages of the finite-time and convergence rate variables offered by

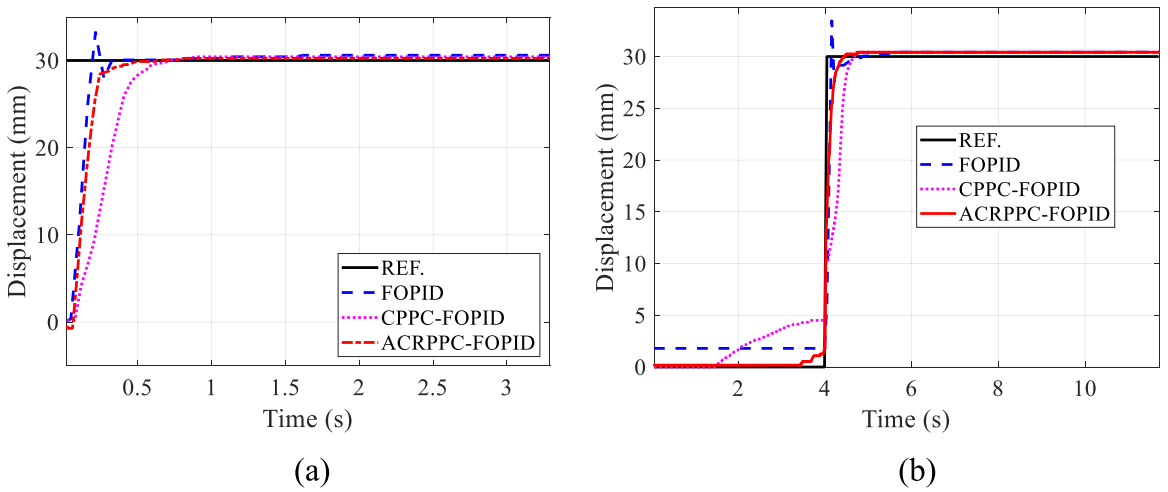

Figure 7. Displacement performance of the rod-piston; (a) Started at 0 second (b) Started at 4 seconds

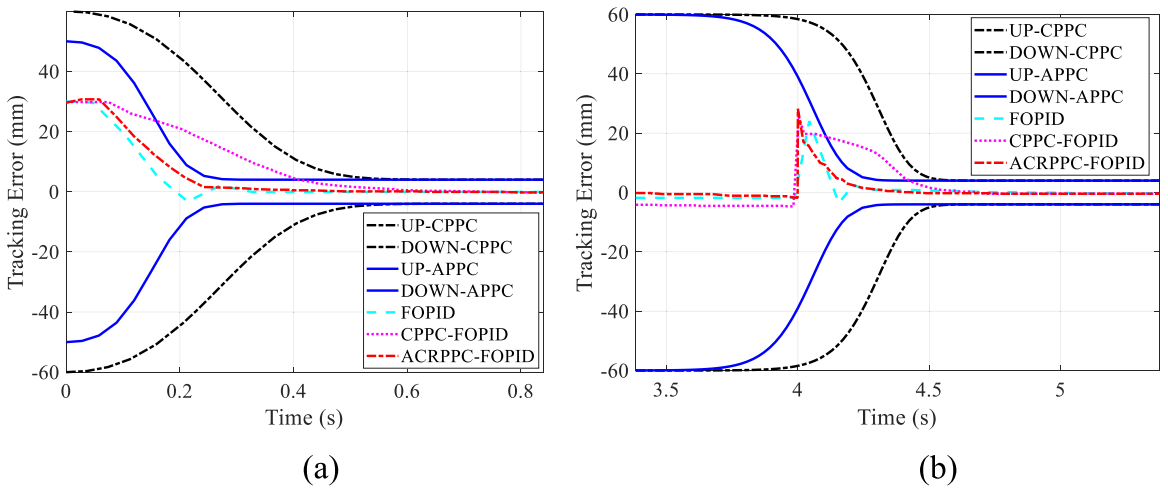

Figure 8. Tracking error performance with prescribed performance bound of the rod-piston started at (a) 0 s and (b) 4 s

the proposed ACRPPC-FOPID in tracking the error of the PPVDC rod-piston. ACRPPC-FOPID reduces the convergence rate period by 0.2s compared to CPPC-FOPID, which results in a 50% reduction in the transient time of the rod-piston with no overshoot, as shown in Fig. 7. In the case of a delayed ignition, only the convergence rate needs to be adjusted to stabilize and improve the rod-piston positioning using ACRPPC-FOPID as seen in Fig. 8(b).

Figs. 7 and 8 indicate that there is a certain impact on the pressure performance in the cylinder, as demonstrated in Fig. 9. In Fig. 9(a), the pressure in the cylinder for ACRPPC-FOPID displays a smooth pressure curve compared to CPPC-FOPID and FOPID. At the initial 0.25 s, ACRPPC-FOPID exhibits very minimal oscillations in pressure, whereas CPPC-FOPID and FOPID show an overshoot of 0 to −1 MPa and fluctuations in pressure. A similar scenario was observed in the delayed ignition operation, as shown in Fig. 9(b). FOPID shows a high overshoot at around 4 s when the positioning starts, which can be linked to the positioning performance depicted in Figs. 7(b) and 8(b), as discussed previously. The results were further substantiated by the tracking performance evaluation using integral absolute error (IAE), integral square error (ISE), and integral time absolute error (ITAE) for a step input trajectory, as shown in Fig. 10. The results indicate that the ACRPPC-FOPID controller exhibits the lowest values of IAE, ISE, and ITAE compared to the FOPID and CPPC-FOPID controllers. ACRPPC-FOPID can achieve about 30% and 2% lower ITAE compared to FOPID and CPPC-FOPID, respectively. Almost similar pattern was recorded for IAE and ISE, whereby ACRPPC-FOPID is slightly lower than CPPC-FOPID and far better than FOPID. These findings suggest that the proposed ACRPPC-FOPID controller consistently provides high tracking performances for nonlinear systems such as PPVDC rod-piston.

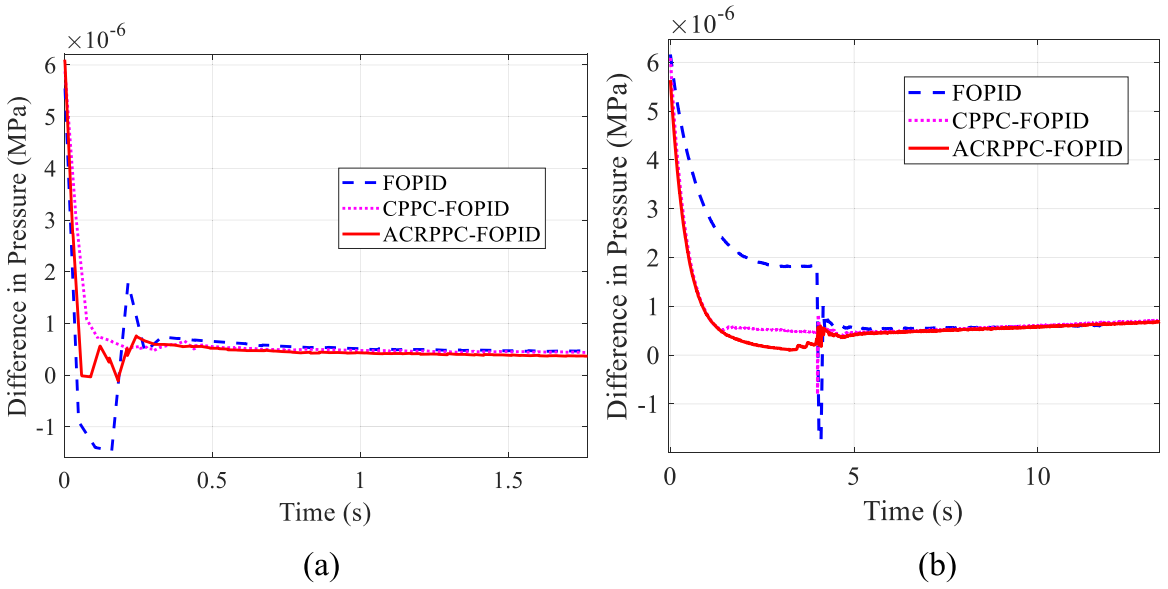

Figure 9. Pressure difference in between both cylinder chambers performances started at (a) 0 s and (b) 4 s

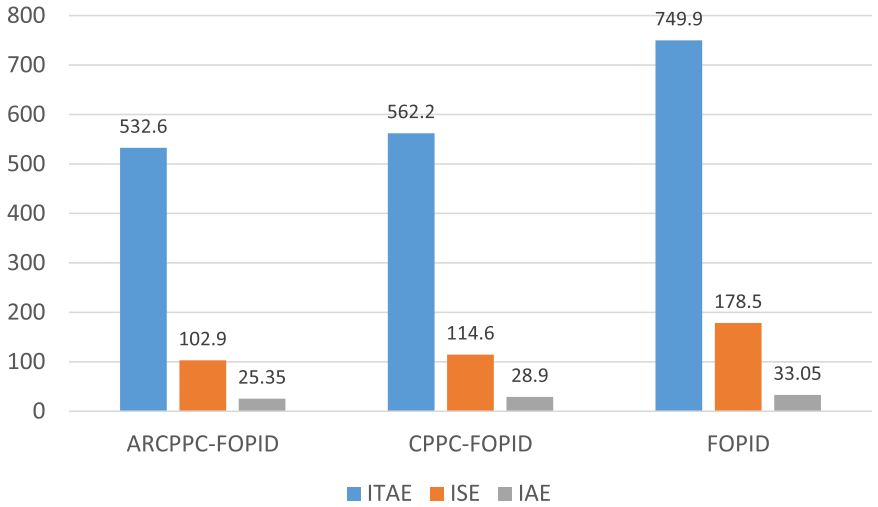

Figure 10. Performance index

Table 4
Controller parameters for sine wave input trajectory test

Controller	Parameters	Value
FOPID (a),(b)	$K_p, K_i, K_d, \lambda, \mu$	435, 68, 7, 0.5, 0.2
ACRPPC-FOPID (a)	$K_p, K_i, K_d, \lambda, \mu,$ $\rho_0, \rho_\infty, \bar{\sigma}, \underline{\sigma}, t_0, \lambda_1, \lambda_2$	65, 0.55, 0.81, 9, 0.1, 50,4,1,1,0.25,1,3
ACRPPC-FOPID (b)	$K_p, K_i, K_d, \lambda, \mu,$ $\rho_0, \rho_\infty, \bar{\sigma}, \underline{\sigma}, t_0, \lambda_1, \lambda_2$	65, 0.55, 0.81, 9, 0.1, 50,4,1,1,0.25,1,3

5.2. Sine Wave Trajectory Test

The validation and analysis were conducted by comparing the FOPID, CPPC-FOPID, and ACRPPC-FOPID controllers with a 0.25-Hz sine wave trajectory, as depicted in Fig. 11. The sine wave trajectory with a frequency of 0.25 Hz was selected because it was the optimal value for experimentation on the targeted test rig. Table 4 displays the controller parameters used for the sine wave input trajectory and its final tuning values. Similar to the step input trajectory test, this experiment was also performed with a 4-s delay ignition.

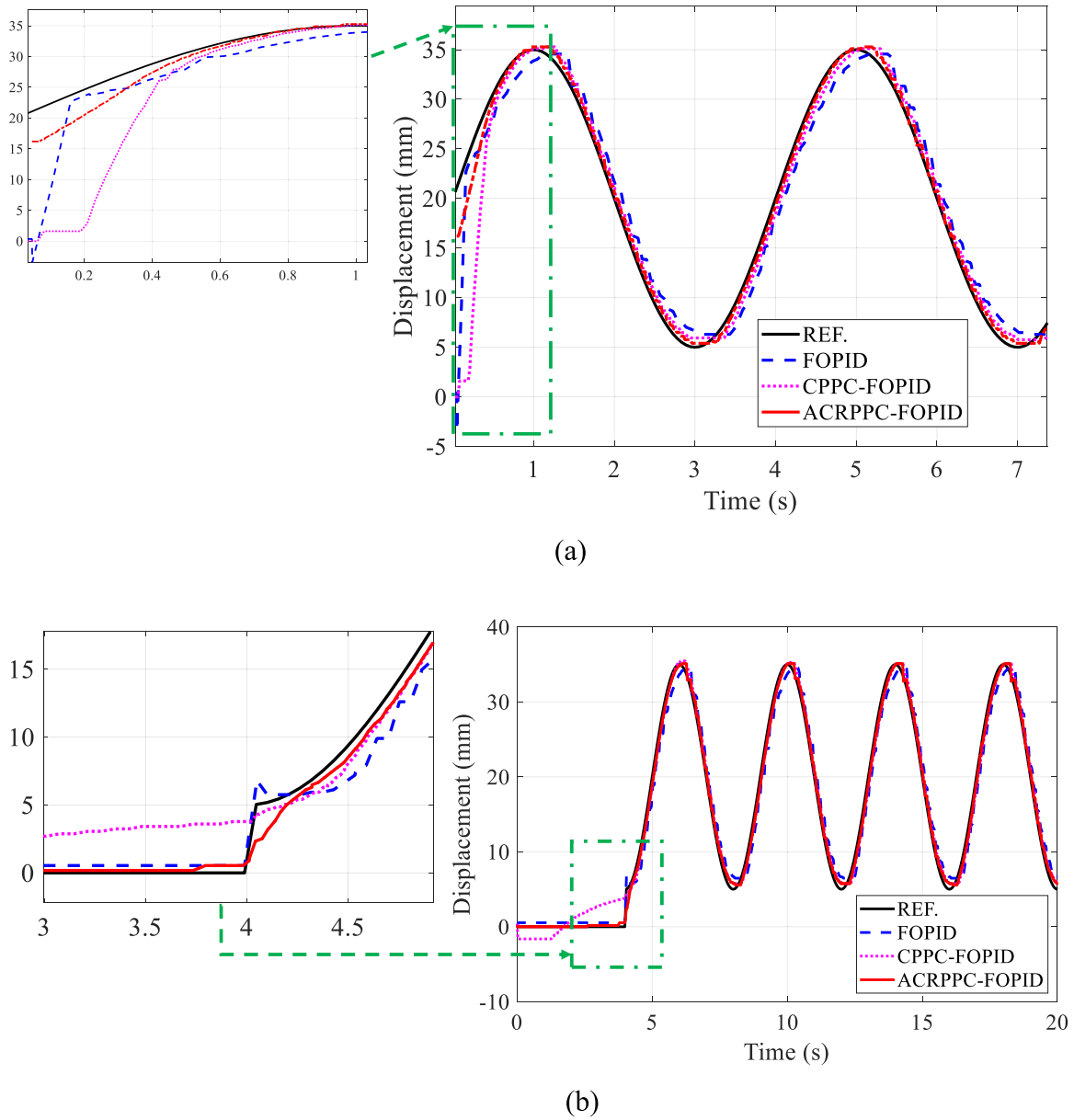

Figure 11. Displacement performance of the rod-piston started at (a) 0 s and (b) 4 s

The ACRPPC-FOPID controller demonstrates smooth operation in its initial stage, when it was deployed with a sine wave trajectory, as shown in Fig. 11. On the other hand, the FOPID controller encountered significant oscillation at the start, as illustrated in Fig. 11(a), and experienced a sharp overshoot that peaked at approximately 4 to 4.2 s, as demonstrated in Fig. 11(b). The performance of the tracking error was influenced by the adjustment of the decay function, as displayed in Fig. 12. After a few cycles of the sine wave trajectory, the tracking error for both the CPPC-FOPID and ACRPPC-FOPID controllers became nearly identical, but they differed in their convergence period. Fig. 12(a) shows that the CPPC-FOPID was delayed by approximately 0.43 s in reaching zero compared to the ACRPPC-FOPID. The AC-PPF's finite-time and convergence rate adjustments resulted in disparities between the ACRPPC-FOPID and CPPC-FOPID, not just in terms of the tracking error but also in the time lag. This difference is evident from the delayed ignition test, as shown in Fig. 11(b) and Fig. 12(b), where the CPPC-FOPID settling time lagged the ACRPPC-FOPID by about 4 s. Meanwhile, the FOPID controller still suffered from oscillation and overshoot, which had an impact on pressure performance, as illustrated in Fig. 13.

Both ACRPPC-FOPID and CPPC-FOPID controllers show minor fluctuations in their pressure behavior during the first rising period, compared to the FOPID controller. The displacement performance, as seen in Fig. 11(a), indicates that during the initial rising phase from 0 to 1 s, the ACRPPC-FOPID maintained nearly constant pressure differences compared to the CPPC-FOPID and FOPID. However,

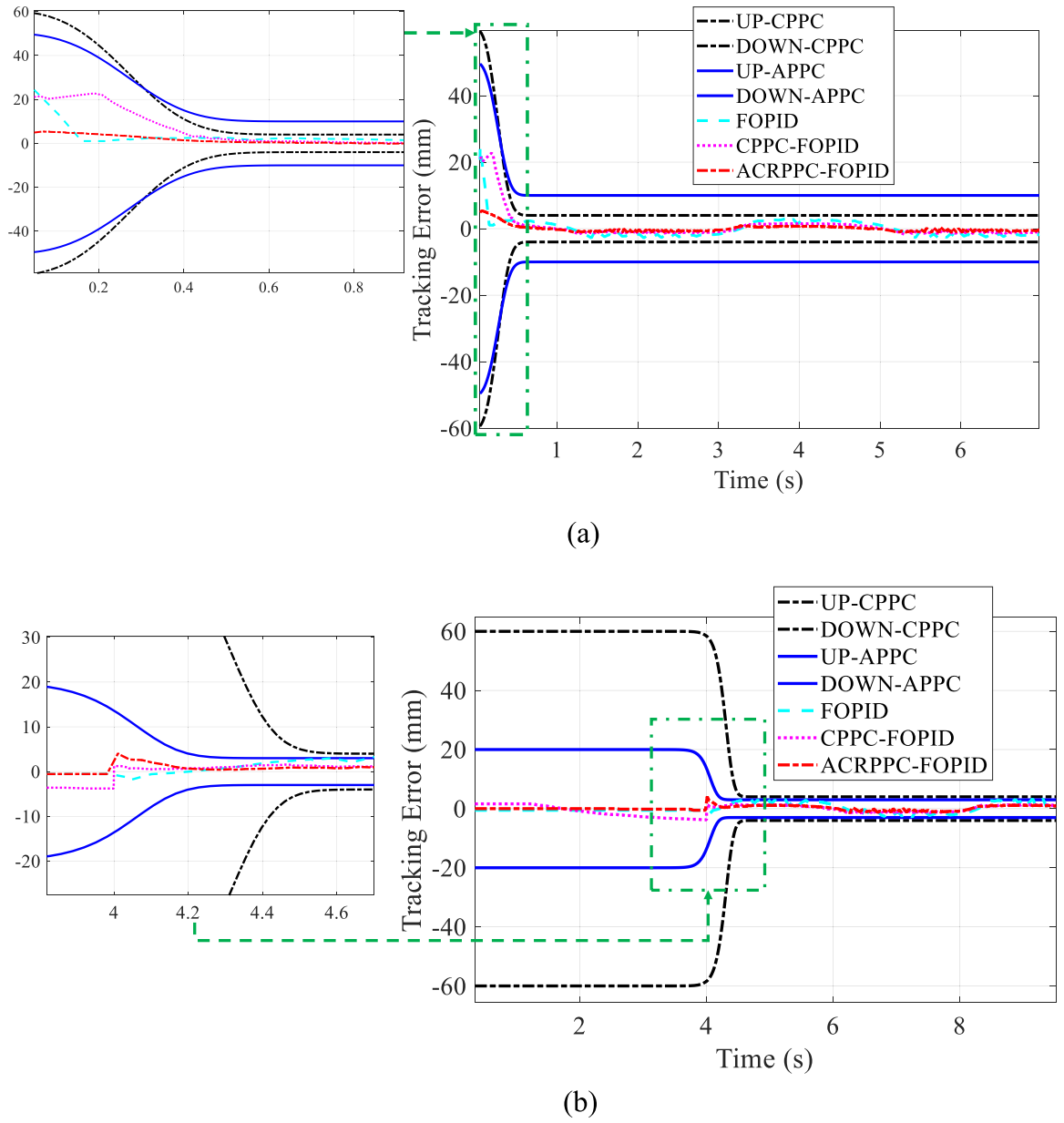

Figure 12. Tracking error performance with prescribed performance bound of the rod-piston started at (a) 0 s and (b) 4 s

a significant negative overshoot was observed at around 0.2 s, as depicted in Fig. 13(a). During the delay ignition test, as shown in Fig. 13(b), the pressure distribution for the CPPC-FOPID was not as smooth as the ACRPPC-FOPID but was much more stable than that of the FOPID. This is due to the impact of gravity force and the friction force between the TPG platform's joint region when the rod-piston expands, pushing the TPG finger downward, and retracts, pulling it upward, during sequential GS and RS operations. This outcome suggests that the ACRPPC-FOPID outperforms both the FOPID and CPPC-FOPID in terms of pressure distribution.

6. Conclusion

The proposed ACR-PPC with FOPID controller strategies were introduced and verified through multiple experiments on the TPG platform, ensuring the system's transient and steady-state error performance. One noteworthy conclusion from this study is that the ACR-PPC effectively eliminates the initial oscillation that leads to mechanical vibration following each rod-piston positioning transient and addresses the phase-shifted issue in the FOPID controller. The improved performance in various input conditions, such as sinusoidal input trajectories, demonstrates that the proposed control strategy can handle the constant time lag or phase shift

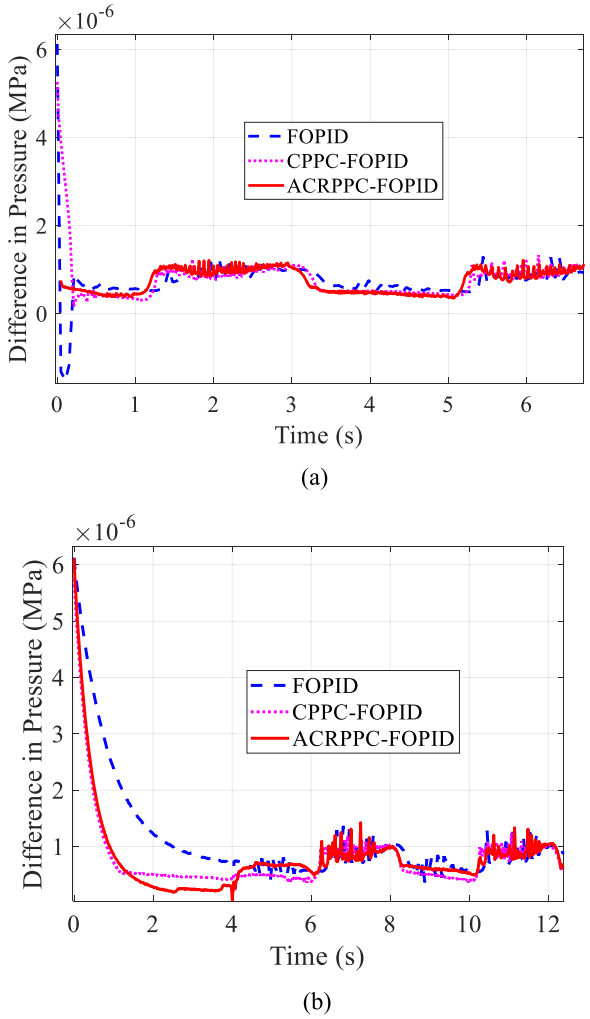

Figure 13. The pressure difference in between both cylinder chambers performance started at (a) 0 s and (b) 4 s

between the desired input and feedback response. Additionally, the absence of approximation in the proposed ACR-PPC reduces the complexity of controller design in terms of methodology. Since pneumatic systems are also known for their highly nonlinear behavior, future research should consider the nonlinear characteristics, such as valve dead-zone, and external disturbances, such as gravity, especially in dynamic and uncertain input conditions.

Declaration of Competing Interest

The authors declare that they have no known competing financial interests or personal relationships that could have appeared to influence the work reported in this paper.

Acknowledgement

The authors would like to thank the Ministry of Higher Education for providing financial support under Fundamental research grant No. FRGS/1/2019/TK04/UMP/02/1 (University reference RDU1901106) and Universiti Malaysia Pahang for laboratory facilities.

Supplementary materials

Supplementary material associated with this article can be found, in the online version, at doi:10.1016/j.cogr.2023.04.004.

References

[1] C.P. Bechlioulis, G.A. Rovithakis, Adaptive control with guaranteed transient and steady state tracking error bounds for strict feedback systems, Automatica 45 (2) (2009) 532–538 2009/02/01/, doi:10.1016/j.automatica.2008.08.012.

[2] C.P. Bechlioulis, G.A. Rovithakis, Robust Adaptive Control of Feedback Linearizable MIMO Nonlinear Systems With Prescribed Performance, IEEE Trans Automat Contr 53 (9) (2008) 2090–2099, doi:10.1109/TAC.2008.929402.
[3] M.I.P. Azahar, A. Irawan, R.M.T.R. Ismail, Self-tuning hybrid fuzzy sliding surface control for pneumatic servo system positioning, Control Eng. Pract. 113 (2021) 104838 2021/08/01/, doi:10.1016/j.conengprac.2021.104838.
[4] V. Nazari, B. Surgenor, Improved position tracking performance of a pneumatic actuator using a fuzzy logic controller with velocity, system lag and friction compensation, Int. J. Control Autom. Syst. 14 (5) (2016) 1376–1388 2016/10/01, doi:10.1007/s12555-015-0202-0.
[5] C. Yin, Y. Cheng, Y. Chen, B. Stark, S. Zhong, Adaptive fractional-order switching-type control method design for 3D fractional-order nonlinear systems, Nonlinear Dyn. 82 (1) (2015) 39–52 2015/10/01, doi:10.1007/s11071-015-2136-8.
[6] A. Ambroziak, A. Chojecki, The PID controller optimisation module using Fuzzy Self-Tuning PSO for Air Handling Unit in continuous operation, Eng. Appl. Artif. Intell. 117 (2023) 105485 2023/01/01/, doi:10.1016/j.engappai.2022.105485.
[7] M.I.P. Azahar, A. Irawan, R. Taufika, Fuzzy Self-Adaptive Sliding Mode Control for Pneumatic Cylinder Rod-Piston Motion Precision Control, J. Phys. Conf. Ser. 1532 (2020) 012028 06/01, doi:10.1088/1742-6596/1532/1/012028.
[8] J. Dong, J. Shi, C. Liu, T. Yu, Research of Pneumatic Polishing Force Control System Based on High Speed On/off with PWM Controlling, Robot Comput Integr Manuf 70 (2021) 102133 2021/08/01/, doi:10.1016/j.rcim.2021.102133.
[9] J. Wang, C. Shao, Y.-.Q. Chen, Fractional order sliding mode control via disturbance observer for a class of fractional order systems with mismatched disturbance, Mechatronics 53 (2018) 8–19 2018/08/01/, doi:10.1016/j.mechatronics.2018.05.006.
[10] H.-.P. Ren, X. Wang, J.-.T. Fan, O. Kaynak, Fractional order sliding mode control of a pneumatic position servo system, J. Franklin Inst. 356 (12) (2019) 6160–6174 2019/08/01/, doi:10.1016/j.jfranklin.2019.05.024.
[11] Q.-.T. Dao, M.-.L. Nguyen, S.-i. Yamamoto, Discrete-Time Fractional Order Integral Sliding Mode Control of an Antagonistic Actuator Driven by Pneumatic Artificial Muscles, Applied Sciences 9 (12) (2019) 2503 [Online]. Available: https://www.mdpi.com/2076-3417/9/12/2503 .
[12] C. Yin, X. Huang, Y. Chen, S. Dadras, S.-m. Zhong, Y. Cheng, Fractional-order exponential switching technique to enhance sliding mode control, Appl Math Model 44 (2017) 705–726 2017/04/01/, doi:10.1016/j.apm.2017.02.034.
[13] H. Wang, Z. Huang, J. Lu, Fractional-order modeling and control of pneumatic-hydraulic upper limb rehabilitation training system, Journal of Intelligent & Fuzzy Systems 39 (2020) 7639–7651, doi:10.3233/JIFS-200891.
[14] Y. Liu, H. Chen, Adaptive Sliding Mode Control for Uncertain Active Suspension Systems With Prescribed Performance, IEEE Transactions on Systems, Man, and Cybernetics: Systems (2020) 1–9, doi:10.1109/TSMC.2019.2961927.
[15] S. Wang, J. Na, Q. Chen, Adaptive Predefined Performance Sliding Mode Control of Motor Driving Systems With Disturbances, IEEE Trans. Energy Convers. (2020) pp. 1-1, doi:10.1109/TEC.2020.3038010.
[16] W. Liu, S. Fei, Q. Ma, H. Zhao, S. Xu, Prescribed performance dynamic surface control for nonlinear systems subject to partial and full state constraints, Appl. Math. Comput. 431 (2022) 127318 2022/10/15/, doi:10.1016/j.amc.2022.127318.
[17] C. Zhang, J. Na, J. Wu, Q. Chen, Y. Huang, Proportional-Integral Approximation-Free Control of Robotic Systems with Unknown Dynamics, IEEE/ASME Trans. Mechatron. (2020) pp. 1-1, doi:10.1109/TMECH.2020.3035660.
[18] P.K. Mishra, P. Jagtap, Approximation-Free Prescribed Performance Control With Prescribed Input Constraints, IEEE Control Systems Letters 7 (2023) 1261–1266, doi:10.1109/LCSYS.2022.3233723.
[19] J. Na, Y. Huang, X. Wu, G. Gao, G. Herrmann, J.Z. Jiang, Active Adaptive Estimation and Control for Vehicle Suspensions With Prescribed Performance, IEEE Trans. Control Syst. Technol. 26 (6) (2018) 2063–2077, doi:10.1109/TCST.2017.2746060.
[20] Y. Liu, Q. Zeng, S. Tong, C.L.P. Chen, L. Liu, Actuator Failure Compensation-Based Adaptive Control of Active Suspension Systems With Prescribed Performance, IEEE Trans. Ind. Electron. 67 (8) (2020) 7044–7053, doi:10.1109/TIE.2019.2937037.
[21] H. Liu, X. Li, X. Liu, H. Wang, Adaptive Neural Network Prescribed Performance Bounded- H-infinity Tracking Control for a Class of Stochastic Nonlinear Systems, IEEE Trans Neural Netw Learn Syst 31 (6) (2020) 2140–2152, doi:10.1109/TNNLS.2019.2928594.
[22] W. Shi, R. Luo, B. Li, Adaptive fuzzy prescribed performance control for MIMO nonlinear systems with unknown control direction and unknown dead-zone inputs, ISA Trans. 66 (2017) 86–95 2017/01/01/, doi:10.1016/j.isatra.2016.08.021.
[23] D. Zhai, C. Xi, L. An, J. Dong, Q. Zhang, Prescribed Performance Switched Adaptive Dynamic Surface Control of Switched Nonlinear Systems With Average Dwell Time, IEEE Transactions on Systems, Man, and Cybernetics: Systems 47 (7) (2017) 1257–1269, doi:10.1109/TSMC.2016.2571338.
[24] M.I.P. Azahar, A. Irawan, and M.S. Ramli, "Transient Control Improvement on Pneumatic Servoing in Robot System using Fractional-Order PID with Finite-time Prescribed Performance Control," in *2022 IEEE 12th Symposium on Computer Applications & Industrial Electronics (ISCAIE)*, 21-22 May 2022 2022, pp. 206–210, doi: 10.1109/ISCAIE54458.2022.9794510.
[25] M.I.P. Azahar and A. Irawan, "Enhancing Precision on Pneumatic Actuator Positioning using Cascaded Finite-time Prescribed Performance Control," in *2021 11th IEEE International Conference on Control System, Computing and Engineering (ICCSCE)*, Penang, Malaysia, 27-28 Aug. 2021 2021, pp. 131–136, doi: 10.1109/ICCSCE52189.2021.9530956.
[26] M.I.P. Azahar, A. Irawan, and M.S. Ramli, "Finite-Time Prescribed Performance Control for Dynamic Positioning of Pneumatic Servo System," in *2020 IEEE 8th Conference on Systems, Process and Control (ICSPC)*, Melaka, Malaysia, 11-12 Dec. 2020 2020, pp. 1–6, doi: 10.1109/ICSPC50992.2020.9305755.
[27] A. Tepljakov, B.B. Alagoz, C. Yeroglu, E. Gonzalez, S.H. HosseinNia, E. Petlenkov, FOPID Controllers and Their Industrial Applications: a Survey of Recent Results, IFAC-PapersOnLine 51 (4) (2018) 25–30 2018/01/01/, doi:10.1016/j.ifacol.2018.06.014.